2026 IEEE International Conference on Robotics and Automation (ICRA 2026)
June 1-5, 2026. Vienna, Austria

Bending Perception-Based Variable Stiffness Control for Snake Robots in Pipe Navigation

Shiyong Meng[1,2], Huizhuo Yang[3], Kai Shen[3], Honglu Xu[3], Gen Chen[3], Jianming Wang[3,4], and Xuan Xiao[3*]

Abstract— **In this paper, Bending Perception-Based Variable Stiffness Control (BP-VSC) is proposed, which enables the snake robot to efficiently navigate complex pipelines. First, the method includes an LSTM-based pipe angle detection model and a control method that transmits a stiffness wave from head to tail. Second, we design a cable-free distributed experimental platform to prevent restrictions caused by cables during pipeline navigation. Finally, a series of experiments are conducted. We optimize the control parameters of BP-VSC in the constructed pipe and evaluated the method. The results demonstrate that BP-VSC significantly enhances the performance of the snake robot in navigating complex pipelines.**

I. INTRODUCTION

In recent years, the field of robotic pipe inspection has gained significant attention due to its potential to enhance the maintenance and safety of pipes. Benefiting from the elongated and flexible body, snake robots have made significant advancements in pipe exploration. However, exploring a complex pipeline with multiple bends remains a challenging task.

To address this issue, compliant control for snake robots has been proposed [1], making the robot adapt to the bends like a spring. In addition, Wang [2] proposed a method utilizing the geometric structure of the robot to reconstruct the required backbone curve, allowing it to match the predefined motion trajectory. Furthermore, Wang [3] proposed a control strategy for snake robots to navigate unstructured environments, enabling adaptation to the surroundings in the forward direction. However, these methods tend to get stuck when encountering larger angle bends.

In addition to adaptive control strategies, precise motion planning strategies for bends have also been studied. Inazawa [4] and Yamada [5] designed specific trajectories for bends using helices stitching, successfully enabling snake robots to navigate through complex pipes. However, such method requires prior knowledge of the environment, and the curve equations involved are relatively complex.

If the shape of the bend can be perceived during motion, the control parameters can be adjusted accordingly to handle bends. Akina [6] added actuators to each joint of the snake robot to adapt to pipes of different diameters. Li [7] proposed a snake robot with contact force sensing that can generate thrust in complex three-dimensional terrain. Rollinson et al. [8] used sensors to determine the robot's pose in real-time, guiding the body to follow a manually specified head direction to navigate turns. However, this strategy relies on human commands that typically require stable video feedback, which can be lost deep within pipes due to communication constraints. In contrast to that work, the method proposed in this paper aims to achieve fully autonomous in-pipe navigation without human guidance.

When we reproduced the experiments of the compliant control, some phenomena caught our attention. First, when the snake robot navigated different types of pipes, the trajectories of joint angles and torque exhibited different patterns. Second, even if the robot got stuck at a right angle bend, one-third of the robot could still pass through the bend. Thus, machine learning can be used to learn the joint angle time series, helping to perceive the pipe environment that the robot is navigating through, and the control parameters can be adjusted for closed-loop control. In summary, the contributions of this paper are as follows:

1) BP-VSC is proposed for snake robots to perceive the bend information of unknown pipes without requiring any additional sensors. BP-VSC can sense the environment by only using joint data, and then adjust the stiffness of each joint accordingly. This method provides a novel idea for sensorless perception for snake robots.
2) A cable-free experimental platform was developed, and extensive experiments were conducted in pipes at various angles. The results validated that the BP-VSC significantly enhances the flexibility of snake robots in navigating pipes while reducing energy consumption.

II. RELATED WORKS

A. Backbone Curve

The helical rolling gait of the snake robot is facilitated by the backbone curve. An approximation method exists between the Frenet-Serret frame and the backbone curve [4], [9].

The backbone curve of the snake robot, modeled within the Frenet-Serret framework, is represented by three orthogonal normalized vectors $(e_1(s), e_2(s), e_3(s))$, where s denotes the arc length parameter. Specifically, $e_1(s)$ indicates the tangent direction, $e_2(s)$ is the principal normal direction, and $e_3(s)$

This work was supported in part by the National Natural Science Foundation of China under Grant 62272489 and in part by the Key Project of Xiangjiang Laboratory under Grant 25XJ02003.

[1]Shiyong Meng is with the School of Computer Science and Engineering, Central South University, Changsha 410083, China.

[2]Shiyong Meng is also with Xiangjiang Laboratory.

[3]Huizhuo Yang, Kai Shen, Honglu Xu, Gen Chen, Jianming Wang, and Xuan Xiao are with Tiangong University, Tianjin, China.

[4]Jianming Wang is also with the Tianjin Key Laboratory of Autonomous Intelligence Technology and Systems, Tianjin, China.

*Xuan Xiao is the corresponding author.

Fig. 1: Snake robot in the pipe.

is the binormal vector. To facilitate the fitting of the snake robot to the backbone curve, a backbone reference frame $(e_r(s), e_p(s), e_y(s))$ is designed, where $e_r(s)$ aligns with $e_1(s)$ to represent the tangent direction of the curve. The vectors $e_p(s)$ and $e_y(s)$ correspond to the pitch and yaw axes, respectively, along the joints of the snake robot. The twist angle $\Phi(s)$ is the angle of rotation between the Frenet-Serret frame and the backbone reference frame around $e_1(s)$, and its calculation formula is given as follows:

$$\Phi(s) = \Phi_0 + \int_0^s \tau(\hat{s}) d\hat{s}, \tag{1}$$

Here, Φ_0 is an arbitrary integration constant representing an initial angle that allows the snake robot to roll along its axis. Additionally, $\tau(s)$ denotes the torsion of the curve at position s, which corresponds to the rate of change of $e_p(s)$ at s.

By adjusting the angles of each joint in real-time, the snake robot can closely follow various segments of the curve throughout its motion cycle, enabling continuous and stable helical rolling. Following the Frenet backbone-curve formulation [4], the desired joint angle of the i-th joint is computed by integrating the curvature over the arc-length interval covered by two adjacent links. Here, l denotes the arc-length distance between two adjacent joints (i.e., the link length in the backbone parameterization), and sh is the shift variable that represents the current phase/position of the robot along the backbone curve. The formula for calculating the joint angles is given by:

$$\theta_i^{\mathrm{d}} = \begin{cases} \int_{\mathrm{sh}-(i-1)l}^{\mathrm{sh}-(i+1)l} -\kappa(s)\sin\Phi(s)\,\mathrm{d}s & \text{(i:odd)} \\ \int_{\mathrm{sh}-(i-1)l}^{\mathrm{sh}-(i+1)l} \kappa(s)\cos\Phi(s)\,\mathrm{d}s & \text{(i:even)} \end{cases} \tag{2}$$

$\kappa(s)$ represents the curvature of the backbone curve at position s, which corresponds to the rate of change of $e_r(s)$ at s.

B. Compliant Control

Due to the complex structure of pipes, traditional position control methods for snake robots are often inadequate. To address this, compliant control is introduced to enhance the robot's adaptability [1], [10]. The goal of compliant control is to maintain a desired dynamic relationship between the robot's motion and the external forces it encounters. This target behavior can be described by a well-established impedance model:

$$M(\ddot{\sigma}_d - \ddot{\sigma}) + K_b(\dot{\sigma}_d - \dot{\sigma}) + K_p(\sigma_d - \sigma) = \tau_{ext} \tag{3}$$

In this model, the left side represents the desired error dynamics, where σ, $\dot{\sigma}$, $\ddot{\sigma}$ are the actual joint angle, velocity, and acceleration, while σ_d, $\dot{\sigma}_d$, $\ddot{\sigma}_d$ are the desired counterparts. M, K_b, K_p are the virtual inertia, damping, and stiffness gains that define the robot's compliance. The term τ_{ext} denotes the torque generated by external environmental forces.

However, fixed impedance parameters (K_p, K_b) are not optimal for all conditions within a pipe. For instance, higher stiffness might be needed for propulsion on smooth surfaces, while lower stiffness is required to navigate cluttered sections. This necessitates an adaptive approach where the robot can perceive its environment and adjust its control parameters accordingly.

C. Time Series LSTM Classification Network

Long Short-Term Memory networks (LSTM) [11], originally introduced by Hochreiter and Schmidhuber, have been widely adopted for sequence modeling tasks due to their ability to overcome the limitations of traditional Recurrent Neural Networks (RNNs).

In time series classification, LSTMs operate by processing sequences of data points over time steps. Each time step updates the network's hidden state while retaining relevant information from previous steps. The ability to dynamically update and store information makes LSTMs ideal for time series data, which often exhibit complex temporal patterns. Vulpi et al. [12] improved terrain classification accuracy by using historical data as input to an LSTM model. This approach enhanced the robot's ability to classify terrain types more precisely by leveraging temporal patterns in the data.

III. Bending Perception-Based Variable Stiffness Control

A. Overview

To improve the performance of the snake robot when navigating complex pipes, we propose a method called BP-VSC. As shown in Fig. 2 , the proposed approach works as follows: the robot inputs the joint angle data from the first five segments into an LSTM model to identify the current pipe's angle. Based on this information, corresponding variable stiffness parameters are applied, and a stiffness wave is transmitted from the head to the tail, aiding the robot in maneuvering through the pipe.

B. Pipe Angle Detection

When the snake robot navigates the bends of the pipe, the first five joints make contact with the pipe, and their joint angles correspond to the bend's curvature. Fig. 2 illustrates our model architecture. The joint data from these five segments is collected at intervals of $\Delta t = 0.05$s and fed into the model. The output is passed through a Softmax layer

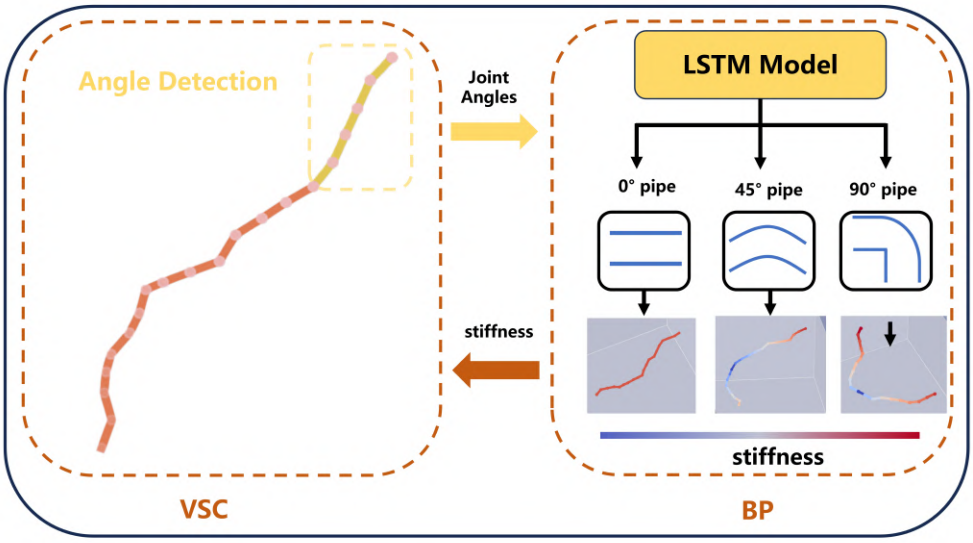

Fig. 2: Overview of the BP-VSC process for navigating through pipes. The snake robot first detects the angle of the current pipe based on the information from the angles of the first five joints. Subsequently, it transmits corresponding stiffness waves backward according to the angle information to facilitate smooth passage through the bends.

Algorithm 1: Algorithm of BP-VSC

Get motor present positions σ_o;
Input σ_o into angle detection model to get pipe angle label θ;
if θ *is* $45°$ **then**
    Propagate a 45° stiffness wave from head to tail at a velocity v;
end if
if θ *is* $90°$ **then**
    Propagate a 90° stiffness wave from head to tail at a velocity v;
end if
Calculate joint torques τ using the stiffness K_p;
Calculate the target joint angles σ_d for the next time step in the helix backbone curve;
Communicate with the motor to set the target angle σ_d and torque τ;

to generate a probability distribution over different angles. The result with the highest probability, provided it exceeds 0.9 and is continuously recognized for more than 2 seconds, is selected as the reliable identification result. If an angle of 45° or 90° is detected, a corresponding stiffness wave is propagated from head to tail.

C. Variable Stiffness Control

When the snake robot reaches a bend in the pipe, the thrust generated by its tail can cause the body to press against the pipe wall at the bend, leading to a blockage. If the entire body were to become too soft, the tail would not be able to generate sufficient forward thrust. Therefore, our variable

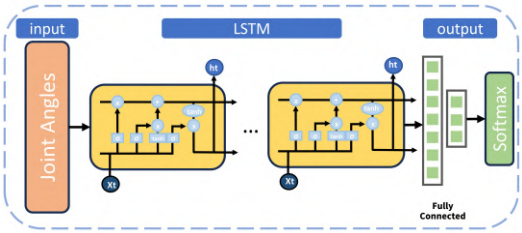

Fig. 3: Model structure of LSTM angle detection model.

stiffness control method reduces the robot's stiffness only at the pipe bends, ensuring smooth passage through the bends.

To ensure the robot's stiffness at the curved regions aligns with its motion, we leverage the snake robot's inherent transmission properties. We employ a Gaussian function-based stiffness wave to modulate the robot's stiffness, ensuring optimized performance in both curved and straight segments of the pipe. The formula for the propagation of a stiffness wave over time can be expressed as:

$$K_v(s,t) = (1-k_m)\cdot\left(1-\exp\left(-\frac{(s-\mu)^2}{2\sigma^2}\right)\right)+k_m \quad (4)$$

$$K_p = K_v * k_n \quad (5)$$

where

$$\mu = v\cdot t \quad (6)$$

$K_v(s,t)$ represents the stiffness at length s along the snake's body at time t, where t is the time since the wave started propagating. k_n and k_m are constants; k_n represents the base stiffness of the snake, and k_m is the minimum value of the stiffness wave. By adjusting σ, the range of stiffness variation along the snake's body can be modified. The parameter v represents the speed at which the stiffness wave

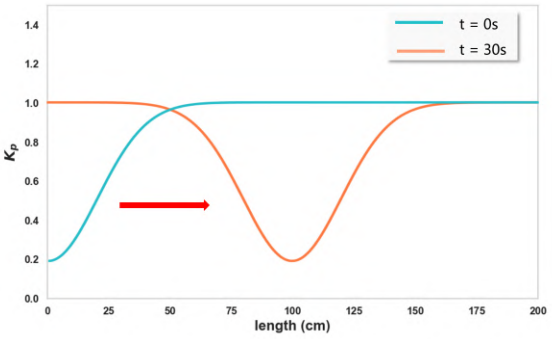

Fig. 4: Initially, the stiffness wave propagates from the head, affecting the joints near the head. At $t = 30$ s, when the snake robot's midsection is at the pipe curvature, the stiffness wave impacts the corresponding section of the robot's body.

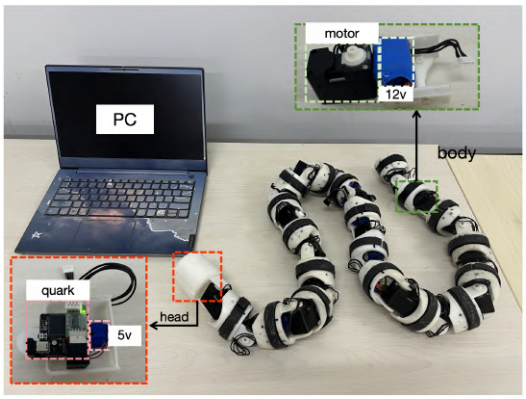

Fig. 5: System implementation of snake robot.

moves along the snake's body. In the experiments, v was set as a constant parameter based on empirical observations of the robot's typical in-pipe speed. Fig. 4 illustrates the propagation of the stiffness wave from 0s to 30s.

It should be noted that the proposed method assumes that the first five segments of the robot do not simultaneously occupy two bends, thereby preventing wave superposition. Consequently, the algorithm is not suitable for helical or continuously curved pipelines. In addition, the current perception module is formulated as a discrete classification problem focusing on standard elbow configurations (45° and 90°), which are commonly found in industrial pipeline systems. Future work will extend the framework toward continuous angle regression and adaptive perception strategies to improve generalization in more complex pipeline environments.

IV. Experimental Platform

A. Snake Robot Structure Design

To validate the effectiveness of the proposed algorithm, we set up an experimental platform. As shown in Fig. 5, each joint of the snake robot is equipped with U-shaped connectors, power supplies, and servo motors. Adjacent structures are connected orthogonally via connectors, enabling the robot to move in both the pitch and yaw directions.

TABLE I: Hardware platform of snake robot.

Control	PC
Power	12.0 V, 3.0A (theoretical max)
Physical Connection	RS-485 Serial
Motor	DYNAMIXEL XH430-W350 Stall Torque: 3.4 N·m Rotate: 180° (Min angle: -90°)
Dimensions (m)	Link: 0.081 Snake: 1.62
Mass(kg)	Total mass: 3.28

B. Hardware Platform

As shown in TABLE I, the robot is equipped with DYNAMIXEL XH430-W350 motors for its joints. The Quark-N, which runs a Linux operating system, was chosen as the main control board and is housed in the head of the robot.

C. Power Supply and Communication

The robot is designed to operate without an external communication and power cable, ensuring that it is not affected by cable interference while navigating long pipes. As illustrated in Fig. 6, each joint motor is powered by an independent 12V battery, which ensures even distribution of the battery weight across the joints and prevents motor failures due to insufficient current. The Quark-N is powered by a 5V battery. Communication with the motors is facilitated through the RS-485 protocol. Due to performance constraints, the angle detection model is deployed on a PC. The main control board transmits angle data to the PC, which then returns the angle detection labels via Wi-Fi.

V. Experimental Results and Analysis

A. Training and Experimentation of the Angle Detection Model

To collect data for building the dataset and training the angle detection model, we conducted 30 sets of experiments in 0°, 45°, and 90° pipes using various stiffness parameters to collect joint angle data from the head of the snake robot as training data. The time series data obtained from inside the pipe were segmented using a window size of 50 and a step size of 5, resulting in 20891 samples.

Based on the previously described model structure, the model utilizes 5 input features corresponding to the first 5 joint angles and incorporates a hidden layer with 64 units to capture temporal dependencies. The architecture includes 4 LSTM layers, which enhance its capacity to model complex

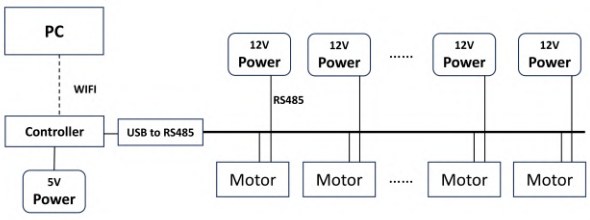

Fig. 6: Power supply and communication design.

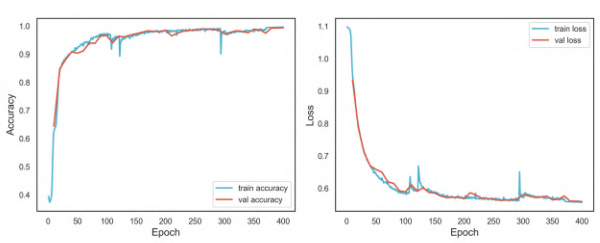

Fig. 7: Training accuracy and loss.

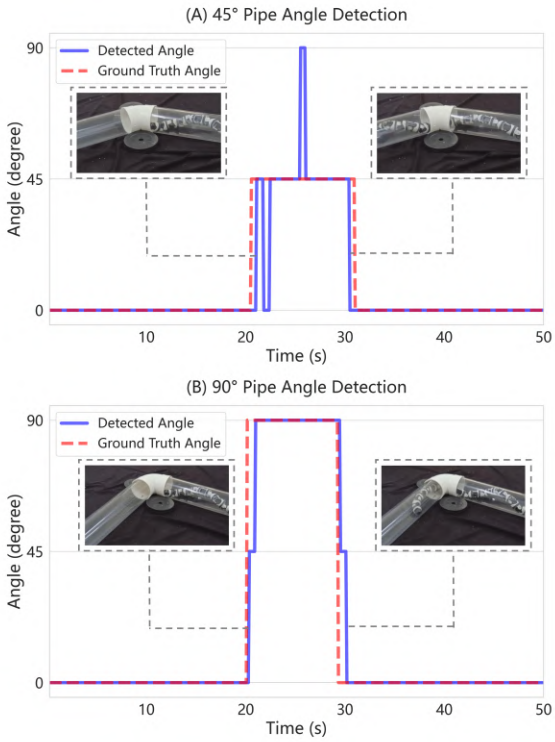

Fig. 8: Angle detection experiments.

sequential patterns. The model was trained for 400 epochs with a batch size of 32 on an RTX 3070 GPU, using the Adam optimizer and cross-entropy loss function, as shown in Fig. 7.

To ensure that the robot can accurately identify the current pipe angle and provide reliable input for subsequent variable stiffness control, we designed an experiment to validate the accuracy of the LSTM model in recognizing pipe angles within complex pipe structures.

Experiments were conducted with the snake robot navigating through pipes with angles of 45° and 90°. The snake robot first navigated a straight section of the pipe before encountering the curved section. Fig. 8A and Fig. 8B illustrate the angle recognition results for a single experiment in each of these scenarios. The blue polyline represents the model-detected angles, while the red polyline represents the ground truth angles. The ground truth angles are defined as the angles from when the first joint of the robot starts to

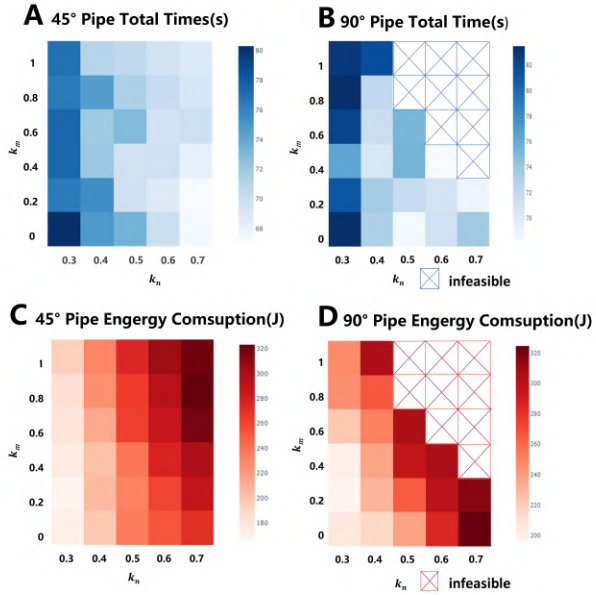

Fig. 9: Experiments on traversal time and energy consumption for the robot passing through pipes.

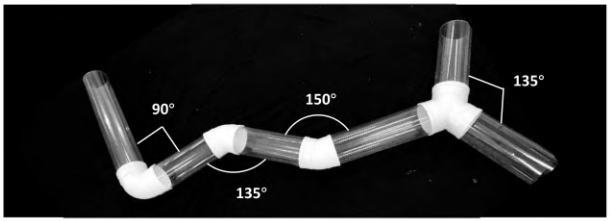

Fig. 10: The setup of the entire pipe.

contact the 45° pipe wall until the fifth joint stops contacting the 45° pipe wall. We present 357 samples from the first 50 seconds.

In the 45° pipe experiment, the robot accurately identified the pipe angle while navigating the straight section. However, upon entering the 45° pipe, some misidentifications occurred due to partial feature overlap between the 0° and 45° pipes. Once the first five joints left the 45° pipe, the model's recognition results stabilized at 0°. The model achieved an accuracy rate of 93.56% across all samples in the 45° pipe experiment.

For the 90° pipe experiment, the model initially misidentified the angle as 45°, but stabilized at 90° shortly afterward. Upon leaving the curved section of the pipe, the model similarly misidentified the angle as 45° before stabilizing at 0°. The model achieved an accuracy rate of 95.24% across all samples in the 90° pipe experiment.

B. Parameter optimization

To demonstrate the impact of different parameters of BP-VSC on its motion characteristics in various pipelines, we conducted extensive experiments, simultaneously proving that BP-VSC can exhibit good performance without the need for meticulous parameter selection. Additionally, we

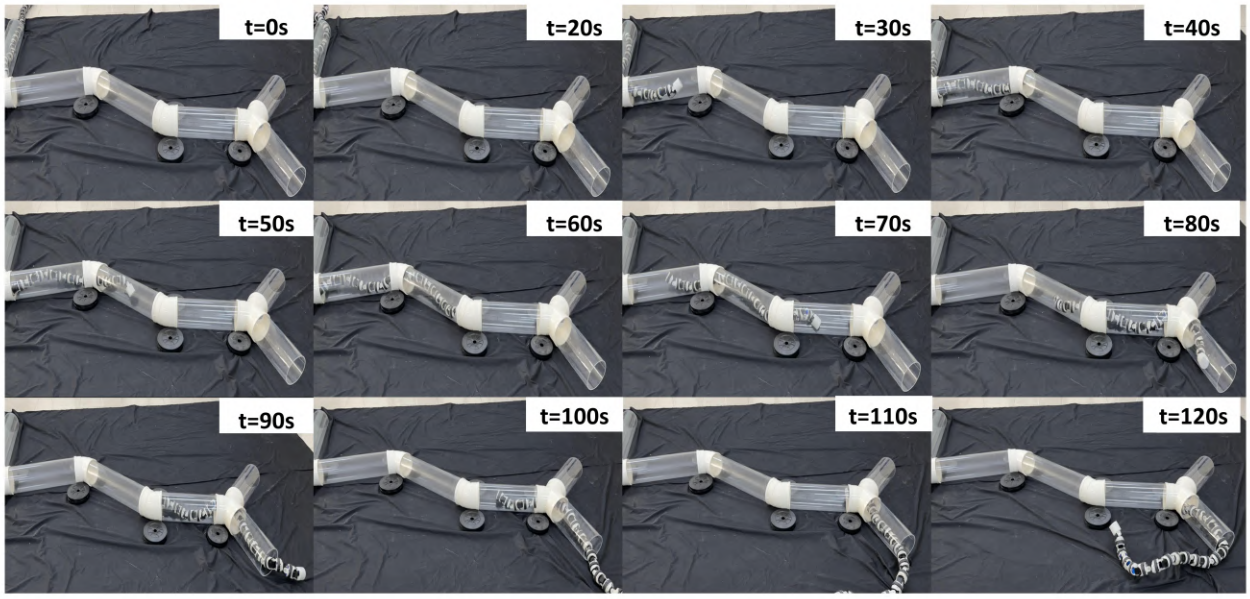

Fig. 11: The experimental process for traversing the entire pipe.

analyzed and optimized the parameter selection from the perspectives of motion time and energy consumption.

Each experiment was recorded from the moment the head of the snake robot entered the pipe until the tail completely exited. We choose total energy consumption and time as the evaluation metrics for the robot's motion performance. The total energy consumption for a single experiment was calculated using the following equation,

$$E = \int_{t_{in}}^{t_{out}} \tau(t) \cdot \omega(t)\, dt \tag{7}$$

$$t_{total} = t_{out} - t_{in} \tag{8}$$

where $\tau(t)$ is the motor torque at time t, and $\omega(t)$ is the angular velocity.

If the robot became stuck or damaged during any trial, the parameter set was considered too risky and classified as *infeasible*. As shown in Fig. 9A, B, in the 90° pipe experiments, 9 out of 30 parameter sets were deemed infeasible.

A larger base stiffness k_n enables the robot to advance more quickly. However, excessive stiffness can cause the robot to become stuck or damaged. In such cases, reducing the stiffness of the robot's body sections inside the pipe by adjusting k_m can help alleviate the forces induced by pipe compression that impede movement. Clearly, when $km = 1$, BP-VSC is disabled, and the algorithm degenerates into impedance control, resulting in a significant decrease in passability and energy consumption.

BP-VSC plays a critical role in reducing energy consumption when the snake robot traverses the pipe. As shown in Fig. 9C, D, both smaller base stiffness k_n and variable stiffness coefficient k_m lead to lower energy consumption. However, excessively low stiffness can result in the robot moving at a significantly slower speed. The selection of optimal parameters balances energy efficiency with speed.

In conclusion, in straight pipes, stiffness variation is unnecessary. For pipes with a curvature of approximately 45°, we set relatively larger values for the stiffness wave parameters k_n and k_m, enabling the robot to traverse these pipes with smaller curvatures more quickly. However, for large-curvature pipes around 90°, we adopt a more conservative parameter strategy, with smaller values of k_n and k_m, to ensure the robot can safely pass through.

C. Entire Pipe Experiment

To validate the effectiveness of the proposed algorithm, we set up a pipeline experimental platform with a total length of 5 meters, as shown in Fig. 10, including pipelines with 90°, 135°, and 150° bends, as well as a Y-shaped configuration to simulate a complex pipeline environment. The 150° bend pipeline is identified as matching the 135° bend. During the experiment, the snake robot identified the pipe angles and adjusted the corresponding stiffness parameters based on the detected angles, allowing it to successfully traverse the entire pipe system.

To evaluate the robustness of the proposed algorithm, 12 complete pipe-navigation experiments were conducted. Among these trials, 10 were successfully completed. The remaining two failures were caused by mechanical disconnections at pipe joints, which were unrelated to the control algorithm itself. Excluding these hardware-related failures, the proposed method achieved successful navigation in all valid trials, demonstrating stable motion performance within the selected parameter range. The control parameters were

chosen as $k_m = 0.3$ and $k_n = 0.5$, which provided a balanced trade-off between motion efficiency and energy consumption. The average traversal speed of the snake robot was measured to be 3.7 cm/s.

VI. Conclusion

In this paper, we propose a Bending Perception-Based Variable Stiffness Control (BP-VSC) method to help snake robots explore unknown pipe environments without the need for additional sensors. We introduce a bending angle perception model based on LSTM, which utilizes joint angle information, along with a variable stiffness control method that softens specific body segments to adapt to pipe bends. A cable-free experimental platform was developed, and extensive experiments were conducted in unknown pipelines. By analyzing the experimental results, we optimized the control parameters for different pipes and successfully navigated a complex 5-meter-long pipe with an experimental success rate of 83%. In future work, we will extend the proposed framework to improve generalization to more complex pipe geometries and strengthen perception-control coupling.

References

[1] M. Travers, J. Whitman, P. Schiebel, D. Goldman, and H. Choset, "Shape-based compliance in locomotion," in *2016 RSS Conference*. RSS, 2016.

[2] T. Wang, J. Whitman, M. Travers, and H. Choset, "Directional compliance in obstacle-aided navigation for snake robots," in *2020 American Control Conference (ACC)*. IEEE, 2020, pp. 2458–2463.

[3] T. Wang, B. Lin, B. Chong, J. Whitman, M. Travers, D. I. Goldman, G. Blekherman, and H. Choset, "Reconstruction of backbone curves for snake robots," *IEEE Robotics and Automation Letters*, vol. 6, no. 2, pp. 3264–3270, 2021.

[4] M. Inazawa, T. Takemori, M. Tanaka, and F. Matsuno, "Unified approach to the motion design for a snake robot negotiating complicated pipe structures," *Frontiers in Robotics and AI*, vol. 8, p. 629368, 2021.

[5] H. Yamada and S. Hirose, "Study of active cord mechanism—approximations to continuous curves of a multi-joint body—," *Journal of the robotics society of japan*, vol. 26, no. 1, pp. 110–120, 2008.

[6] A. Kuwada, S. Wakimoto, K. Suzumori, and Y. Adomi, "Automatic pipe negotiation control for snake-like robot," in *2008 IEEE/ASME International Conference on Advanced Intelligent Mechatronics*. IEEE, 2008, pp. 558–563.

[7] D. Ramesh, Q. Fu, and C. Li, "Sensnake: A snake robot with contact force sensing for studying locomotion in complex 3-d terrain," in *2022 International Conference on Robotics and Automation (ICRA)*. IEEE, 2022, pp. 2068–2075.

[8] D. Rollinson and H. Choset, "Pipe network locomotion with a snake robot," *Journal of Field Robotics*, vol. 33, no. 3, pp. 322–336, 2016.

[9] W. Huang, X. Guo, H. Liu, and Y. Fang, "A robust model-based radius estimation approach for helical climbing motion of snake robots," *IEEE/ASME Transactions on Mechatronics*, vol. 28, no. 6, pp. 3284–3293, 2023.

[10] D. Rollinson, K. V. Alwala, N. Zevallos, and H. Choset, "Torque control strategies for snake robots," in *2014 IEEE/RSJ International Conference on Intelligent Robots and Systems*. IEEE, 2014, pp. 1093–1099.

[11] S. Hochreiter and J. Schmidhuber, "Long short-term memory," *Neural computation*, vol. 9, no. 8, pp. 1735–1780, 1997.

[12] F. Vulpi, A. Milella, R. Marani, and G. Reina, "Recurrent and convolutional neural networks for deep terrain classification by autonomous robots," *Journal of Terramechanics*, vol. 96, pp. 119–131, 2021.